Journal of Materials Chemistry A

ROYAL SOCIETY OF CHEMISTRY

PAPER

View Article Online
View Journal | View Issue

Check for updates

Cite this: J. Mater. Chem. A, 2022, 10, 6065

# Single Mo atoms paired with neighbouring Ti atoms catalytically decompose ammonium bisulfate formed in low-temperature SCR†

Junxiao Chen,[a] Xue Fang,[a] Zhouhong Ren,[b] Weiye Qu,[a] Xiaolei Hu,[a] Zhen Ma,[ac] Liwei Chen,[b] Xi Liu,*[b] Yaxin Chen *[a] and Xingfu Tang *[acd]

Received 25th September 2021
Accepted 31st October 2021

DOI: 10.1039/d1ta08269h

rsc.li/materials-a

Selective catalytic reduction (SCR) of $NO_x$ with $NH_3$ has been widely used for $NO_x$ emission control, but commercial catalysts inevitably suffer severe deactivation in $SO_2$-containing stack gases at low temperatures because the ammonium bisulfate ($NH_4HSO_4$, ABS) formed in SCR blocks the surface active sites. We resolve this issue by developing a $TiO_2$-supported single-atom Mo catalyst ($Mo_1/TiO_2$) that decomposes ABS at ~225 °C, far lower than the dew point of ABS (~260 °C). Single Mo atoms paired with the neighboring surface Ti atoms function as Mo–Ti acid–base dual sites, which respectively adsorb the $NH_4^+$ and $HSO_4^-$ of ABS. After the oxidation of $NH_4^+$ by surface lattice oxygen on the Mo sites, electrons left behind on the dual sites are localized around the Fermi level, which allows them to transfer to the adsorbed $HSO_4^-$ on the Ti sites, thus releasing $SO_2$ at low temperatures. The $Mo_1/TiO_2$ catalyst with Mo–Ti acid–base dual sites enables the decomposition of ABS at low temperatures, and thus this work provides a way to effectively control $NO_x$ emission particularly from industrial boilers.

Published on 01 novembris 2021. Downloaded on 31.07.2024 03:51:10.

## 1 Introduction

Nitrogen oxides ($NO_x$) emitted from mobile and stationary sources are not only major atmospheric pollutants, but also important precursors for the formation of ozone and secondary aerosols,[1,2] and hence are severely harmful to human health and the environment. With the increasingly stringent environmental regulations, enormous efforts have been devoted to controlling $NO_x$ emissions.[3,4] Selective catalytic reduction (SCR) of $NO_x$ with $NH_3$ over $V_2O_5$-based catalysts is the state-of-the-art technology for abating $NO_x$ emission from high-temperature (300–400 °C) stack gases.[5,6] Nevertheless, these catalysts will inevitably suffer severe deactivation when this technology is applied in low-temperature and $SO_2$-containing stack gases typically from many industrial boilers, largely because the surface catalytic sites are covered by viscous ammonium bisulfate ($NH_4HSO_4$, ABS) formed in SCR.[7–9] Hence, it is necessary to develop low-temperature ABS-resistant catalysts to ensure that SCR catalysts efficiently operate under such conditions.

There are two main strategies to develop low-temperature ABS-resistant catalysts on the basis of the formation mechanism of ABS and its properties. One can be defined as a source-controlling strategy. ABS is formed mainly from two sequential reactions, *i.e.*, $SO_2 + 1/2\ O_2 \rightarrow SO_3$ and $SO_3 + H_2O + NH_3 \rightarrow NH_4HSO_4$,[10] and thus the formation of ABS can be avoided by preventing the oxidation of $SO_2$ to $SO_3$. To slow down the reaction rate of $SO_2$ oxidation, adjusting the redox properties of catalysts such as by lowering the loading of active components seems feasible.[9,11] However, this strategy is not optimal because the lower reaction rate of $SO_2$ oxidation is at the expense of the low SCR activity.[12] Meanwhile, there is often a certain amount of $SO_3$ in flue gases, which makes the formation of ABS inevitable by the reaction of $SO_3$ with $NH_3$ and $H_2O$.

The other strategy is to develop SCR catalysts with a function of decomposing ABS at low temperatures. ABS deposited on active sites is reported to be usually decomposed in a relatively high temperature range owing to its viscosity and the electrostatic attraction between $NH_4^+$ and $HSO_4^-$.[13–15] Two kinds of interaction are often important factors to determine the temperatures required for ABS decomposition: ABS-catalyst adsorption interactions and $NH_4^+$–$HSO_4^-$ electrostatic interactions. Conventional methods are often focused on the interactions between ABS and catalysts and thus the lowest decomposition temperature for ABS was reported to be ~340 °C.[16–19] Nevertheless, an extremely strong electrostatic interaction between $NH_4^+$ and $HSO_4^-$ exists in ABS,[20] making

[a]Department of Environmental Science & Engineering, Fudan University, Shanghai, 200438, P. R. China. E-mail: tangxf@fudan.edu.cn; 16110740025@fudan.edu.cn
[b]School of Chemistry and Chemical, In-situ Center for Physical Science, Shanghai Jiao Tong University, Shanghai, 200240, P. R. China. E-mail: liuxi@sjtu.edu.cn
[c]Shanghai Institute of Pollution Control and Ecological Security, Shanghai, 200092, P. R. China
[d]Jiangsu Collaborative Innovation Centre of Atmospheric Environment & Equipment Technology, Nanjing University of Information Science & Technology, Nanjing, 210044, P. R. China

† Electronic supplementary information (ESI) available. See DOI: 10.1039/d1ta08269h

Published on 01 novembris 2021. Downloaded on 31.07.2024 03:51:10.

the low-temperature decomposition of ABS to produce $SO_2$ and $N_2$ unfavorable.[21] To address that challenge, our previous work successfully broke the electrostatic interaction by spatially separating $NH_4^+$ from $HSO_4^-$ with the assistance of layered $MoO_3$, which allows electron transfer between separated $NH_4^+$ and $HSO_4^-$ mediated by catalysts, thus achieving a lower decomposition temperature of ABS at ~275 °C.[22] However, limited by the weak interaction between acidic $MoO_3$ and $HSO_4^-$,[23] this decomposition temperature is still high (higher than the reported lowest dew point of ABS, ~260 °C).[24] Therefore, dual sites for $NH_4^+$ and $HSO_4^-$ adsorption and strong electron transfer ability are key requirements for catalysts to effectively decompose ABS at low temperatures.

Considering the adsorption model of ABS previously reported,[25] a desired catalyst should possess acid–base dual sites to adsorb $NH_4^+$ and $HSO_4^-$, respectively. The electron transfer from $NH_4^+$ to $HSO_4^-$ on that catalyst should be realized through the oxidation of $NH_4^+$ on the acid site together with the reduction of $HSO_4^-$ on the base site by electrons left behind on the acid–base dual sites. It was reported that $MoO_3$ has strong acidity to adsorb the $NH_4^+$ of ABS and the ability to oxidize $NH_4^+$,[26,27] while the $TiO_2$ support surfaces can provide the basic sites for adsorbing the acidic $HSO_4^-$ of ABS.[27,28] Hence, a catalyst with Mo–Ti acid–base dual sites should readily adsorb $NH_4^+$ and $HSO_4^-$, respectively. Moreover, owing to the unsaturated coordination configuration, the surface Mo ions often have the desired ability to facilitate the oxidation of $NH_4^+$,[29] generating reduced Mo species. Due to the charge transfer between Mo and Ti atoms *via* $Mo^{5+} + Ti^{4+} \rightarrow Mo^{6+} + Ti^{3+}$,[30] the produced $Ti^{3+}$, which often has a higher electron state density near the Fermi level ($E_f$),[31] favourably accelerates the reduction of $HSO_4^-$. What is more, it is feasible to fabricate the Mo–Ti acid–base dual sites because Mo species tend to disperse on the surface of $TiO_2$ in the form of Mo single atoms,[32] which can pair with neighboring Ti sites to form acid–base dual sites.

In this work, we developed a $TiO_2$-supported single-atom Mo catalyst ($Mo_1/TiO_2$), which can decompose ABS at temperatures far lower than the dew point of ABS. Based on systematic characterization *via* density functional theory (DFT) calculation, aberration-corrected scanning transmission electron microscopy (AC-STEM), Raman spectroscopy, diffuse-reflectance infrared Fourier-transform (DRIFT) spectroscopy, Fourier transform infrared spectroscopy (FT-IR) and X-ray photoelectron spectroscopy (XPS), atomically dispersed Mo adatoms on the surface of $TiO_2$ resulted in the formation of abundant Mo–Ti dual sites, which respectively adsorb the $NH_4^+$ and $HSO_4^-$ of ABS. Further electron transfer from $NH_4^+$ to $HSO_4^-$ mediated by these Mo–Ti dual sites was realized, resulting in $Mo_1/TiO_2$ decomposing ABS at a temperature as low as ~225 °C. This work proposes a strategy for designing ABS-resistant catalysts to effectively control $NO_x$ emissions particularly from industrial boilers.

# 2 Experimental

## 2.1 Catalyst preparation

Titanium oxide ($TiO_2$, 5–10 nm) was obtained from Shanghai Aladdin Biochemical Technology Co., Ltd. Ammonium molybdate tetrahydrate ($(NH_4)_6Mo_7O_{24}\cdot 4H_2O$) and ammonium bisulfate ($NH_4HSO_4$, ABS) were acquired from Sinopharm Chemical Reagent Co., Ltd (China).

In a typical synthesis, a precursor solution was prepared by dissolving 0.147 g $(NH_4)_6Mo_7O_{24}\cdot 4H_2O$ into 20 mL deionized water under stirring. Then 2.0 g $TiO_2$ was added and the slurry was evaporated to dryness in a water bath at 80 °C, accompanied by drying in an oven at 80 °C for 12 h. The powder was then calcined at 550 °C for 3 h to get 6 wt% $MoO_3/TiO_2$ (denoted as $Mo_1/TiO_2$ catalyst). Besides, 0.40 g $TiO_2$ was further loaded on 1.0 g $Mo_1/TiO_2$ by impregnation and the obtained solid was calcined at 550 °C for 3 h to acquire the $TiO_2/Mo_1/TiO_2$ catalyst.

As for $MoO_3/TiO_2$ catalysts with a series of $MoO_3$ loadings on $TiO_2$, they were synthesized by tuning the amount of $(NH_4)_6Mo_7O_{24}\cdot 4H_2O$ added to 0.073, 0.098, 0.123, 0.490, 0.736, or 0.981 g, respectively, following the same procedure used for the preparation of the $Mo_1/TiO_2$ catalyst. For 0.5 or 2 wt% ABS-loaded samples, 0.005 or 0.02 g ABS was dissolved in 20 mL deionized water and 1.0 g of the corresponding catalyst was added later. After evaporating to dryness at 80 °C in a water bath and drying at 80 °C for 12 h, ABS-deposited catalysts were obtained.

In order to better understand the electron transfer pathway, the $Mo_1/TiO_2$ catalyst was further treated by (i) $NH_4^+$ oxidation: the catalyst was pre-reduced under 50 mL $min^{-1}$ 3 vol% $NH_3$/He for 3 h followed by a 50 mL $min^{-1}$ Ar atmosphere for another 3 h at 230 °C; (ii) $HSO_4^-$ reduction: 2 wt% ABS was loaded on the catalyst and the obtained sample was then treated at 300 °C for 3 h under a 500 mL $min^{-1}$ $N_2$ flow; (iii) re-oxidation: the catalyst obtained in step (ii) was oxidized at 300 °C for 3 h under a 500 mL $min^{-1}$ mixed 3 vol% $O_2$ + 97 vol% $N_2$ flow.

## 2.2 Catalyst characterization

X-ray diffraction (XRD) patterns of the catalysts were collected *via* a Rigaku D/MAX2200V X-ray diffractometer at 40 kV and 40 mA using Ni-filtered Cu Kα radiation ($\lambda = 0.15418$ nm). Transmission electron microscopy (TEM, JEOL JEM-2100F) and high-resolution TEM (HRTEM) were recorded using a JEOL JEM-2100F transmission electron microscope. Besides, AC-STEM images and energy dispersive X-ray spectroscopy (EDX) measurements were performed on a probe-corrected scanning/transmission electron microscope (Thermo Fisher Thermis Z) equipped with a SuperEDX detector at an accelerating voltage of 300 kV. An XploRA confocal spectrometer (Jobin Yvon, Horiba Gr, France) was used to obtain Raman spectra. The Raman scattering was excited by an external-cavity diode (785 nm) and coupled with a 50× Olympus microscope objective (Olympus, 0.50 numerical aperture). The power of the laser was 9 mW. The Raman spectra were collected at a resolution of 3 $cm^{-1}$ with two accumulations at a 10 s acquisition time using a 1200 lines per mm diffraction grating. To analyze the change in electron states after a series of treatments, XPS was performed on a Kratos Axis Ultra DLD system with a monochromatic Al-Kα X-ray gun (1486.6 eV). Spectra were calibrated by adjusting the C 1s peak to 284.6 eV. XPSPEAK 4.1 with a Shirley-type background was used to analyze and process XPS data. DRIFT

 This journal is © The Royal Society of Chemistry 2022

Published on 01 novembris 2021. Downloaded on 31.07.2024 03:51:10.

spectroscopy of $NH_3$ adsorption was conducted by accumulating 64 scans at 4 $cm^{-1}$ resolution from 4000 to 1000 $cm^{-1}$ on a Nicolet IS 50 Fourier transform infrared spectrometer equipped with a Harrick Scientific DRIFT cell and a mercury-cadmium-telluride MCT/A detector. After the catalyst was pretreated at 300 °C for 1 h to remove physically adsorbed water and trace residues in a flow of $N_2$ (150 mL $min^{-1}$) and then cooled to 50 °C, the background spectra were collected under a $N_2$ flow. Then, the $NH_3$ adsorption on the catalysts was achieved by exposing the catalysts to a flow of 500 ppm $NH_3/N_2$ (150 mL $min^{-1}$) at 50 °C for 1 h. After removing physically adsorbed $NH_3$ in a flow of $N_2$ (150 mL $min^{-1}$) for 1 h, the DRIFT spectra were collected with background correction. To observe the evolution of ABS on the surface of the catalyst, *in situ* DRIFTS was carried out. In order to remove the physically adsorbed water, pretreatment of the catalysts was undertaken in a flow of $N_2$ (50 mL $min^{-1}$) at 200 °C for 1 h. Then the temperature was raised to 260 °C and the $N_2$ flow was changed to 25 mL $min^{-1}$. The DRIFT spectra were collected with 4 $cm^{-1}$ resolution and 64 scans between 4000 and 1000 $cm^{-1}$ every two minutes. As for the FT-IR spectra of 0.5 wt% ABS-deposited samples, they were mixed with KBr at a ratio of 1 : 99, pressed, and dried under infrared light. The spectra were obtained with 4 $cm^{-1}$ resolution and 64 scans between 4000 and 1000 $cm^{-1}$.

### 2.3 Catalytic evaluation

All the above-synthesized catalysts were pressed, crushed, and sieved to 40–60 mesh for evaluation. Temperature-programmed decomposition (TPDC) experiments were performed in a fixed-bed quartz reactor (inner diameter of 6 mm) and detected using a Fourier-transform infrared spectrometer (Thermo Scientific Antaris IGS analyzer) under atmospheric pressure. Before TPDC experiments, 2 wt% ABS was loaded on the surface of each catalyst. During the test, 0.20 g sample was used and the $N_2$ flow rate was 500 mL $min^{-1}$ with a temperature ramp of 5 °C $min^{-1}$. A temperature-programmed procedure was adopted to record the temperature data.

$NH_3$ oxidation experiments were performed and $NH_3$ oxidation was detected using the same instrument as in TPDC experiments. In $NH_3$ oxidation experiments, 0.50 g catalyst was used, and the gas flow rate was 500 mL $min^{-1}$, containing 500 ppm $NH_3$, 3 vol% $O_2$, and balanced $N_2$. The temperature ramp was 2 °C $min^{-1}$.

The stability experiment of $Mo_1/TiO_2$ was evaluated at 260 °C in the same reactor used for the TPDC experiments, and the gas exiting the reactor was analyzed with an online chemiluminescence NO–$NO_2$–$NO_x$ analyzer (42i-HL, Thermo Fisher Scientific, Waltham, MA). During the test, 0.50 g catalyst was used and the gas flow was 500 mL $min^{-1}$, containing 3 vol% $O_2$, 500 ppm NO, 500 ppm $NH_3$, 500 ppm $SO_2$, 5 vol% $H_2O$, and balanced $N_2$.

### 2.4 Density functional theory (DFT) calculations

All the spin polarized DFT + U calculations were performed using the VASP program with PW91 potentials, and the effective U for Ti 3d orbitals was set to be 4.2 eV. Self-consistence of the electronic energy is reached when the energy change is smaller than $10^{-5}$ eV. The force of each free atom converged to 0.03 eV $Å^{-1}$ during geometric optimization. Besides, a 2 × 2 × 1 Monkhorst–Pack *k*-point grid was used for Brillouin zone sampling.

## 3 Results and discussion

Anatase $TiO_2$ (101) was selected as the exposed surface to anchor single Mo atoms because it is often the mainly exposed plane,[33] and thus a $Mo_1/TiO_2$ model was constructed by using the DFT method to scheme the decomposition of ABS at low temperatures, as shown in Fig. 1a. A single Mo atom was fixed on $TiO_2$ (101) since $MoO_3$ tends to atomically disperse on the surface of $TiO_2$.[32,34] This acidic Mo atom (yellow ball in Fig. 1a) pairs with the neighboring surface basic Ti atom (blue ball in Fig. 1a) to form Mo–Ti acid–base dual sites, which respectively adsorb the $NH_4^+$ and $HSO_4^-$ of ABS *via* acid–base interactions. Following the oxidation of $NH_4^+$ on Mo sites, electrons left on the Mo–Ti dual sites transfer to the Ti sites, where the reduction of $HSO_4^-$ occurs and $SO_2$ desorbs from the surface and is released.

In order to shed light on the charge transfer ability of Mo–Ti dual sites, DFT calculations were performed to evaluate the electronic state of Mo and Ti in the pristine $Mo_1/TiO_2$ catalyst and the reduced one ($Mo_1/TiO_2$–R) by removing a linked oxygen in Mo–Ti dual sites to simulate the situation after $NH_4^+$

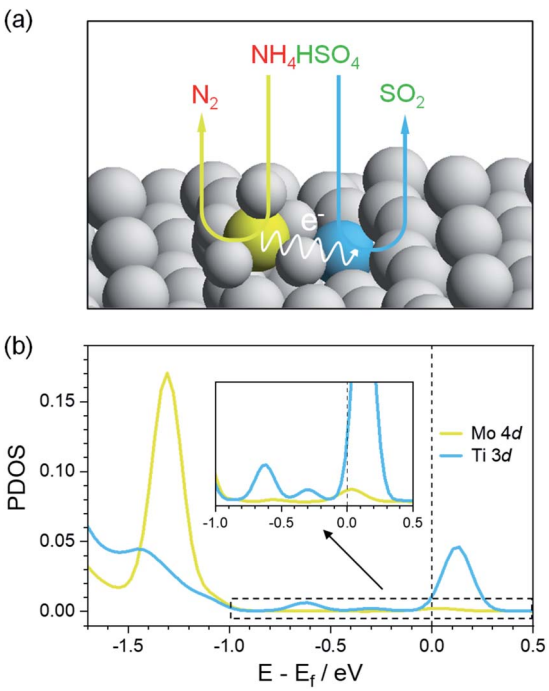


Fig. 1 (a) Schematic diagram of the decomposition pathway of ABS over $Mo_1/TiO_2$. A single Mo atom (yellow ball) pairs with a Ti neighbour (blue ball) to form a Mo–Ti dual site, where the $NH_4^+$ of ABS is adsorbed and oxidized on Mo sites, while $HSO_4^-$ is attached to and reduced on Ti sites. The wave-type arrow represents a possible electron transfer pathway between those two sites. (b) PDOS of the Mo site (4d) and Ti site (3d) in $Mo_1/TiO_2$–R.

Published on 01 novembris 2021. Downloaded on 31.07.2024 03:51:10.

oxidation, and the projected density of states (PDOS) results are shown in Fig. 1b and S2.† For the pristine structure, both Ti 3d and Mo 4d showed peaks at ~−0.9 eV (Fig. S2†), indicating the strong hybridization between Mo and Ti together with the bridging O atom, implying easy electron transfer between Mo and Ti.[35] After the $NH_4^+$ oxidation by the Mo site, the finite density of states at the Fermi level emerged for Ti 3d due to higher occupancy of d orbitals.[36] These electrons at the Fermi level possessed a greater electron-donating capacity which may be favorable for reducing $HSO_4^-$ by transferring these high-energy charges to the anti-bonding orbitals of $HSO_4^-$. Therefore, such Mo–Ti dual sites can realize electron transport from $NH_4^+$ to $HSO_4^-$ and thus the decomposition of ABS at low temperatures theoretically.

To verify the feasibility of this strategy, we synthesized a $Mo_1/TiO_2$ catalyst and explored the structure of Mo species on the surface of $TiO_2$. No peak assigned to $MoO_3$ appears on the XRD pattern of $Mo_1/TiO_2$, revealing a highly dispersed state of Mo ions on the surface of anatase $TiO_2$ (Fig. S3†). A similar phenomenon was observed by TEM, *i.e.*, no $MoO_3$ particle was detected on $TiO_2$ (Fig. S4†). Meanwhile, the EDX mapping image of $Mo_1/TiO_2$ displayed in Fig. 2b showed highly dispersed Mo ions. Furthermore, single Mo atoms dispersed on $TiO_2$ (101) were clearly observed in the AC-STEM image of $Mo_1/TiO_2$ (Fig. 2c). As further analyzed by the two-dimensional simulated images of the selected area shown in Fig. 2d and the calculated structural model in Fig. S1,† single Mo atoms with a $MoO_5$ motif were established. One Mo atom is bound to two twofold coordinated O atoms of $TiO_2$ and two introduced hydroxy which link a Mo adatom and two fivefold coordinated Ti atoms, and one Mo=O dangling bond points away from the surface.[32] These single Mo atoms coordinating with surrounding Ti atoms facilitate the formation of abundant Mo–Ti dual sites.

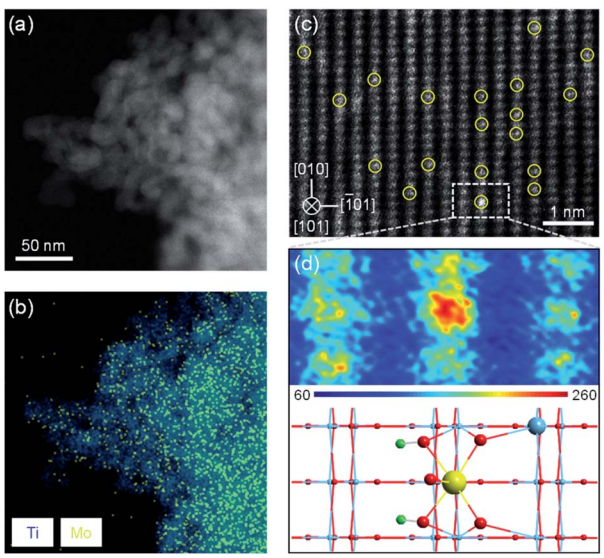


Fig. 2 (a) AC-STEM and (b) EDX mapping images of $Mo_1/TiO_2$. (c) Atomic-resolution AC-STEM image of $Mo_1/TiO_2$. (d) Two-dimensional simulated image (above) and the corresponding structural model (below) of the selected area in (c). Light blue represents Ti atoms, red O atoms, green H atoms, and yellow Mo atoms.

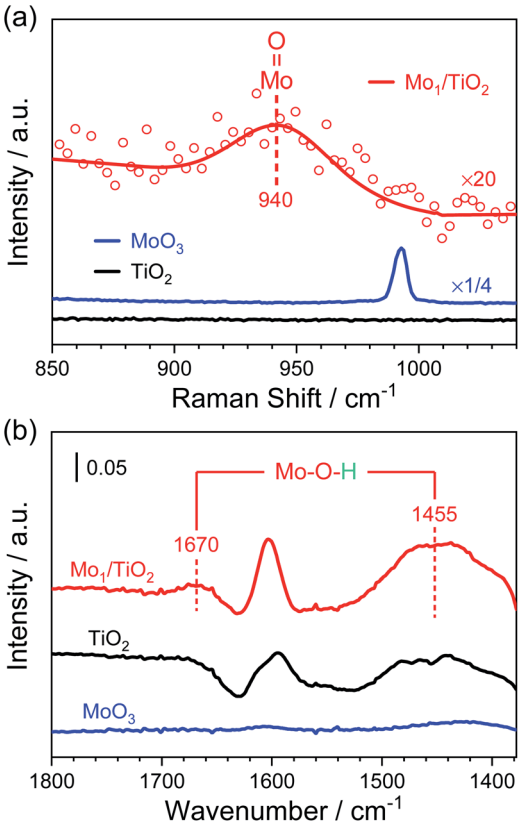


Fig. 3 (a) Raman spectra and (b) $NH_3$-DRIFT spectra of $Mo_1/TiO_2$, $MoO_3$ and $TiO_2$ catalysts.

Furthermore, Raman spectra and $NH_3$-DRIFT spectra were collected to determine the configuration of Mo atoms. In Fig. 3a, a small shoulder at ~940 $cm^{-1}$ appears in the Raman spectrum of $Mo_1/TiO_2$ compared with that of $TiO_2$. As reported, surface molybdenum oxide species possess the terminal Mo=O Raman stretching in the range of 934–954 $cm^{-1}$, while the peak shifted to higher frequency for bulk $MoO_3$,[37] indicating the existence of a dangling Mo=O bond. In the Raman spectrum of $Mo_1/TiO_2$, no specific signal can be observed at ~875 $cm^{-1}$ or ~820 $cm^{-1}$ assigned to the stretching mode of a Mo–O–Mo bond in surface or bulk molybdenum oxide species, respectively (Fig. S6†), evidencing the existence of single Mo atoms, in line with the results in Fig. 2. As for the $NH_3$-DRIFT spectra shown in Fig. 3b, only a peak at ~1600 $cm^{-1}$ assigned to the adsorbed gas $NH_3$ on Lewis sites appears in the spectrum of $TiO_2$.[29] However, when single Mo atoms were anchored on $TiO_2$, significant signals at ~1670 and ~1455 $cm^{-1}$ appeared, manifesting the increased $NH_3$ coordination of Brønsted sites in the form of $NH_4^+$,[29,38] *i.e.*, Mo–O–H structures were formed on the surface of $Mo_1/TiO_2$, which are totally different from that in bulk $MoO_3$ where no relevant peak was observed. As a result, Mo single sites provide a particular Mo–O–H matrix for $NH_4^+$ adhesion.

For the purpose of estimating the behaviour of adsorbed $NH_4^+$ on the Mo–Ti dual sites, $NH_3$ oxidation experiments were implemented on $Mo_1/TiO_2$, $MoO_3$ and $TiO_2$. As shown in Fig. 4a, the onset of the $NH_3$-oxidation curves of $Mo_1/TiO_2$ located at

 This journal is © The Royal Society of Chemistry 2022

Published on 01 novembris 2021. Downloaded on 31.07.2024 03:51:10.

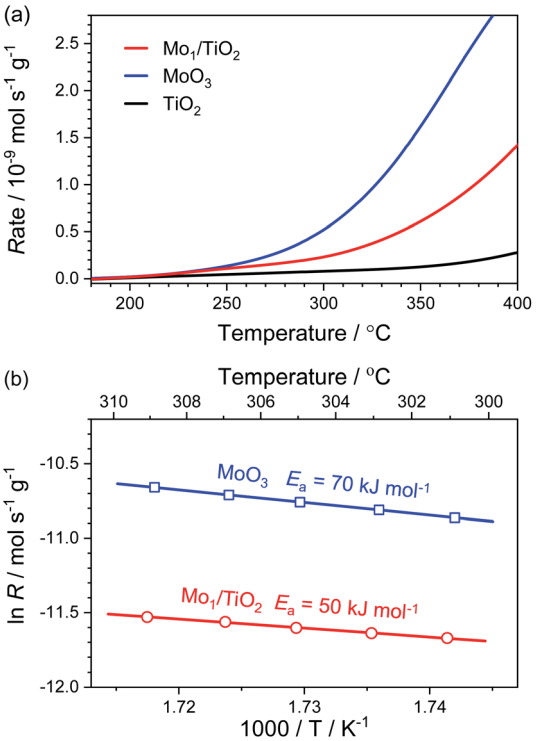


Fig. 4 (a) Reaction rates of the $NH_3$ oxidation as a function of temperature over $Mo_1/TiO_2$, $MoO_3$ and $TiO_2$. (b) Arrhenius plots for reaction rates with $E_a$ over $Mo_1/TiO_2$ and $MoO_3$.

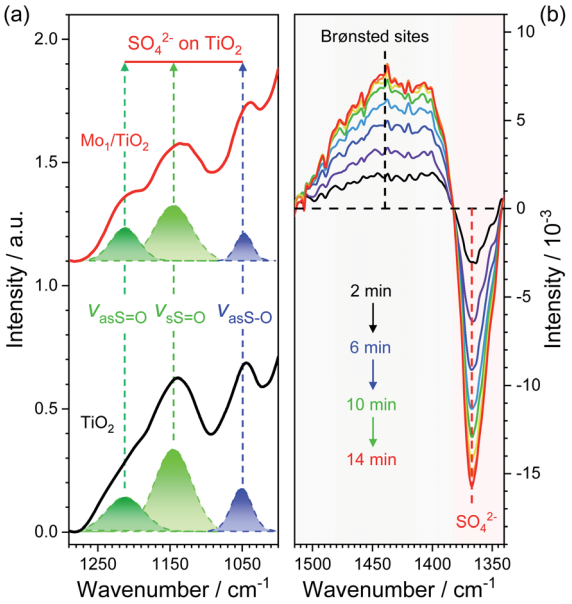


Fig. 5 (a) FT-IR spectra of ABS-deposited $TiO_2$ and $Mo_1/TiO_2$. (b) *In situ* DRIFT spectra of the transient reaction on the 0.5% ABS-deposited $Mo_1/TiO_2$ catalyst at 260 °C. The initial spectrum was deducted as the background.

~200 °C, reflecting a strong ability of $Mo_1/TiO_2$ towards $NH_3$ oxidation. Similarly, $MoO_3$ started to catalyse $NH_3$ oxidation at ~200 °C, the same as $Mo_1/TiO_2$, while the onset temperature shifted to ~300 °C for $TiO_2$, showing that the Mo atoms of the dual sites are responsible for $NH_3$ oxidation. Fig. 4b shows the Arrhenius plots for the rate ($R$) of $NH_3$ oxidation together with activation energy ($E_a$) over $Mo_1/TiO_2$ and $MoO_3$. The $E_a$ of $Mo_1/TiO_2$ is 50 kJ $mol^{-1}$, much lower than that of $MoO_3$ (70 kJ $mol^{-1}$), suggesting a strong interaction between Mo single atoms and neighboring Ti atoms which activates the surface lattice oxygen of Mo. Thus, combined with the results obtained from $NH_3$-DRIFT spectra, the Mo atoms of Mo–Ti dual sites should be responsible for the adsorption and oxidation of $NH_4^+$ in ABS.

Based on the dual-site adsorption model of ABS,[25] it is likely that $HSO_4^-$ adsorbs on the neighboring Ti sites in consideration of $NH_4^+$ adsorption on Mo sites. FT-IR spectra were used to detect surface structures of catalysts after ABS deposition (Fig. 5a and S7†). For pure ABS, peaks at ~1242, 1172, and 1072 $cm^{-1}$, assigned to the bending vibrations of SO–H ($\delta_{SO-H}$), symmetrical stretching vibrations of S=O ($\nu_{sS=O}$), and asymmetrical stretching vibrations of S–O ($\nu_{asS-O}$) in $HSO_4^-$ emerged, respectively.[28] After ABS was loaded on the surface of $MoO_3$, only slight changes occur in the position of the peaks, demonstrating weak interactions between $MoO_3$ and $HSO_4^-$. In contrast, the FT-IR spectra of ABS-deposited $TiO_2$ and $Mo_1/TiO_2$ are both quite different from that of pure ABS. Both spectra have peaks at ~1222 and 1134 $cm^{-1}$ corresponding to the asymmetrical stretching vibrations of S=O ($\nu_{asS=O}$) and $\nu_{sS=O}$, respectively, and a peak at ~1042 $cm^{-1}$ ($\nu_{asS-O}$).[28] The similar spectral features between the spectra of ABS-loaded $TiO_2$ and $Mo_1/TiO_2$ illustrate that $HSO_4^-$ is adsorbed on surface exposed Ti sites. Moreover, the disappearance of $\delta_{SO-H}$ and the appearance of $\nu_{asS=O}$ in the spectra of $Mo_1/TiO_2$ compared to pure ABS indicates the transformation of $HSO_4^-$ into $SO_4^{2-}$,[23] *via* a strong interplay between $TiO_2$ and $HSO_4^-$. The interaction resulted in obvious redshifts of $\nu_{asS-O}$, indicating the increase of the S–O bond length and hence the reduction of its bonding energy,[39] which is favorable for the cleavage of two S–O bonds of $SO_4^-$ so as to release $SO_2$. Hence, the co-adsorption of $NH_4^+$ and $HSO_4^-$ of ABS on acid–base Mo–Ti dual sites was established, where Mo sites and Ti sites are responsible for the oxidation of $NH_4^+$ and the reduction of $HSO_4^-$, respectively.

To confirm whether such Mo–Ti dual sites realize low-temperature decomposition of ABS, the dynamic evolution of ABS on $Mo_1/TiO_2$ through time-resolved DRIFT spectra was observed to directly depict the decomposition process on the Mo–Ti dual sites (Fig. 5b). The strong peak at ~1363 $cm^{-1}$ could be assigned to $SO_4^{2-}$,[40] which gradually faded (here is the inversed peak becoming stronger and stronger with time), indicative of the decomposition of ABS. In contrast, the peak between ~1500 and 1380 $cm^{-1}$ characterized to be $NH_4^+$ adsorbed on Brønsted sites gradually increased.[41] According to the decomposition equation of ABS: $NH_4HSO_4 \rightarrow 1/3\ NH_3 + 1/3\ N_2 + SO_2 + 2\ H_2O$,[21] one third of the $NH_4^+$ species are eventually released in the form of $NH_3$, and the formed $NH_3$ will be adsorbed on the regenerated Brønsted sites, explaining the increase of signal between ~1500 and 1380 $cm^{-1}$ in Fig. 5b. Consequently, it is evident that the Mo–Ti dual sites indeed facilitate the decomposition of ABS at low temperatures.

Published on 01 novembris 2021. Downloaded on 31.07.2024 03:51:10.

According to the above decomposition equation of ABS, we further determined the onset temperature for the decomposition of ABS by conducting TPDC experiments on catalysts pre-reduced in the $NH_3/N_2$ atmosphere (Fig. S8–S10†). The results from TPDC are shown in Fig. 6a. The onset temperature for pure ABS decomposition was measured to be ~350 °C. Note that for $Mo_1/TiO_2$, the onset temperature greatly decreased down to a temperature as low as ~225 °C, while the corresponding onset temperatures for $TiO_2$ and $MoO_3$ are ~350 and ~275 °C, respectively. These results indicate that the catalytic sites for the low-temperature decomposition of ABS on $Mo_1/TiO_2$ are the Mo–Ti dual sites rather than surface standalone Mo or Ti sites. For reference, we deposited ABS with the same loading on a conventional $V_2O_5$–$WO_3/TiO_2$ (VWTi) catalyst, and found that the onset temperature was ~300 °C. This result is consistent with the fact that high decomposition temperature determined that conventional $V_2O_5$–$WO_3/TiO_2$ catalysts used at thermal plants often effectively operate only at temperatures higher than 300 °C. Otherwise, these catalysts will suffer deactivation.[4] In contrast, $Mo_1/TiO_2$ can decompose ABS at temperatures as low as 225 °C, far lower than the reported lowest dew point of ABS.[15] Because both Mo and Ti of $Mo_1/TiO_2$ are also important components of commercial $V_2O_5$–$MoO_3/TiO_2$ SCR catalysts, $Mo_1/TiO_2$ provides a crucial base for designing strong ABS-resistant SCR catalysts typically applied in many industrial boilers, as further confirmed by the high stability of the $Mo_1/TiO_2$ catalyst under simulation stack gas conditions of industrial boilers (Fig. S11†). Meanwhile, based on the results from TPDC experiments, the yield rates of $SO_2$ were also calculated (Table S1†), and $Mo_1/TiO_2$ exhibited the highest yield rate, revealing a strong ability towards the decomposition of ABS.

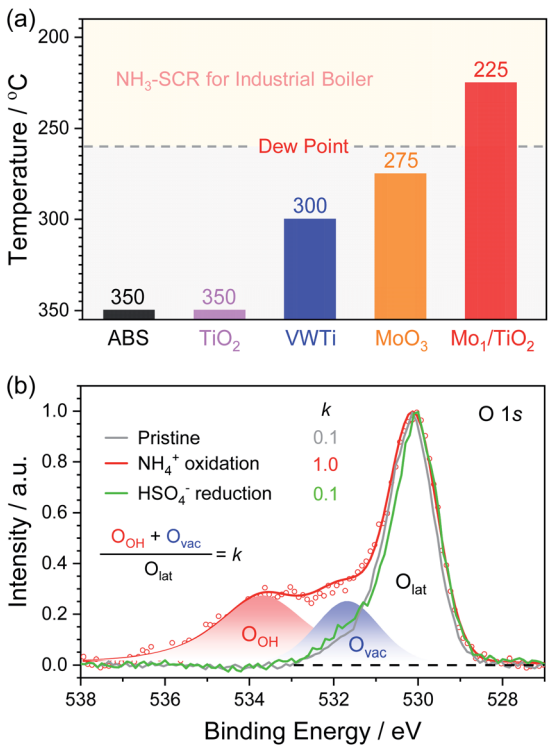


Fig. 6 (a) Onset temperatures of the $SO_2$ release over a series of ABS-deposited catalysts. (b) O 1s XPS of $Mo_1/TiO_2$ (pristine and after $NH_4^+$ oxidation and $HSO_4^-$ reduction).

The release of $SO_2$ during TPDC reflects the reduction of $HSO_4^-$ by the Mo–Ti dual sites. Hence, the decomposition process of ABS can be divided into three stages: $NH_4^+$ oxidation, $HSO_4^-$ reduction, and re-oxidation of the catalyst by $O_2$. XPS was adopted to probe the evolution of electron states of the pristine $Mo_1/TiO_2$ catalyst and those after each stage (Fig. 6b and S12†). After $NH_4^+$ oxidation, the ratio of $Mo^{5+}$ increased from 41% to 64%, clearly confirming the electron transfer from $NH_4^+$ to single Mo atoms. Simultaneously, the ratio of oxygen vacancies ($O_{vac}$) to surface lattice oxygen ($O_{lat}$) increased dramatically. Note that a new high-energy peak at 533.6 eV in the XPS of Fig. 6b related to oxygen in O–H ($O_{OH}$) appeared after the $NH_4^+$ oxidation, consistent with the increase of the Brønsted sites in Fig. 5b. As illustrated in Fig. 1b, after the formation of oxygen vacancies *via* the oxidation of $NH_4^+$ on the Mo–Ti dual sites, electronic state densities of both Ti and Mo ions emerged at the Fermi level in Ti 3d and Mo 4d orbitals of the dual sites, which readily transfer to $HSO_4^-$ adsorbed on the Ti site. Moreover, the protons of the Brønsted sites also play an important role in transferring charge between Mo and Ti ions of the dual sites,[42] which is beneficial to the reduction of $HSO_4^-$ and subsequent release of the produced $SO_2$. Again, due to the desorption of $SO_2$ concomitant with the $H_2O$ release resulting from the reduction of $HSO_4^-$, the remaining oxygen atoms filled the oxygen vacancies, accounting for the decrease of $O_{vac}$ (Fig. 4b). Accompanied by the re-oxidation process, all the electronic states were eventually restored to the original states (Fig. S12†), completing the decomposition of ABS on the $Mo_1/TiO_2$ catalyst.

The above discussion demonstrates that single Mo atoms with neighboring Ti atoms function as Mo–Ti dual sites which provide Mo sites for the adsorption and oxidation of $NH_4^+$, and Ti sites for the adsorption and reduction of $HSO_4^-$. In order to further verify the effect of Mo–Ti dual sites in the decomposition process of ABS, we adjusted the surface structure of the catalyst by tuning the Mo loading or wrapping the exposed Mo single atoms with $TiO_2$. The decomposition temperature remains basically stable (~225 °C) at low Mo loadings, but increases to another constant (~260 °C) at high loadings which is closer to that of bulk $MoO_3$ (Fig. S13 and S14†). Meanwhile, further coverage of $TiO_2$ also resulted in the delay of the temperature for the $SO_2$ release (Fig. S15†). Therefore, the Mo–Ti acid–base dual sites, namely the pair of single Mo atom and neighboring Ti atom, are key to the decomposition of ABS over $Mo_1/TiO_2$ at low temperatures.

## 4 Conclusions

In summary, we designed a $Mo_1/TiO_2$ catalyst to solve the problem of ABS poisoning on low-temperature SCR catalysts. The $Mo_1/TiO_2$ catalyst successfully achieved the decomposition of ABS at ~225 °C, which is superior to that of other catalysts reported previously. With various characterization techniques such as XRD, TEM, Raman and AC-STEM, single Mo atoms on $TiO_2$ were defined, ensuring the formation of Mo–Ti acid–base

 This journal is © The Royal Society of Chemistry 2022

Published on 01 novembris 2021. Downloaded on 31.07.2024 03:51:10.

dual sites by single Mo atoms pairing with the neighboring surface Ti atoms, which respectively adsorb the $NH_4^+$ and $HSO_4^-$ of ABS, as confirmed by DRIFT and FT-IR spectra. After the oxidation of $NH_4^+$ by the surface lattice oxygen on the Mo sites, electrons left behind on the dual sites are localized around the Fermi level, which allows them to transfer to the adsorbed $HSO_4^-$ on the Ti sites, releasing $SO_2$ at low temperatures. Therefore, this work proposed a strategy for designing ABS-resistant catalysts for effectively controlling $NO_x$ emission particularly from industrial boilers.

## Author contributions

X. T., Y. C. and X. L. conceived and directed the research. J. C. conducted the experiments of catalyst preparation and evaluation, and performed the experimental characterization. X. F. conducted the DFT calculations. J. C., Z. R., W. Q., X. H., L. C. and Z. M. discussed the results and wrote the manuscript. All authors have given approval to the final version of the manuscript.

## Conflicts of interest

There are no conflicts to declare.

## Acknowledgements

This work was financially supported by the National Natural Science Foundation of China (21976037, 21777030) and the National Engineering Research Center for Synergetic Control of Air Pollutants and Greenhouse Gases (NEL-KF-201903).

## Notes and references

1 J. H. Seinfeld, *Science*, 1989, **243**, 745–752.
2 S. C. Anenberg, J. Miller, R. M. Injares, L. Du, D. K. Henze, F. Lacey, C. S. Malley, L. Emberson, V. Franco, Z. Klimont and C. Heyes, *Nature*, 2017, **545**, 467–471.
3 S. Reis, P. Grennfelt, Z. Klimont, M. Amann, H. ApSimon, J. P. Hettelingh, M. Holland, A. C. LeGall, R. Maas, M. Posch, T. Spranger, M. A. Sutton and M. Williams, *Science*, 2012, **338**, 1153–1154.
4 L. P. Han, S. X. Cai, M. Gao, J. Hasegawa, P. L. Wang, J. P. Zhang, L. Y. Shi and D. S. Zhang, *Chem. Rev.*, 2019, **119**, 10916–10976.
5 M. H. Zhu, J. K. Lai, U. Tumuluri, M. E. Ford, Z. L. Wu and I. E. Wachs, *ACS Catal.*, 2017, **7**, 8358–8361.
6 N. Y. Topsøe, *Science*, 1994, **265**, 1217–1219.
7 S. Matsuda, T. Kamo, A. Kato, F. Nakajima, T. Kumura and H. Kuroda, *Ind. Eng. Chem. Prod. Res. Dev.*, 1982, **21**, 48–52.
8 P. Forzatti and L. Lietti, *Heterog. Chem. Rev.*, 1996, **3**, 33–51.
9 G. Busca, L. Lietti, G. Ramis and F. Berti, *Appl. Catal., B*, 1998, **18**, 1–36.
10 C. Y. Zhou, L. N. Zhang, Y. Deng and S. C. Ma, *Environ. Prog. Sustainable Energy*, 2016, **35**, 1664–1672.
11 H. Zhao, S. Bennici, J. Cai, J. Shen and A. Auroux, *Catal. Today*, 2010, **152**, 70–77.
12 P. Forzatti, *Catal. Today*, 2000, **62**, 51–65.
13 L. Y. Song, J. D. Chao, Y. J. Fang, H. He, J. Li, W. G. Qiu and G. Z. Zhang, *Chem. Eng. J.*, 2016, **303**, 275–281.
14 Y. Z. Xi, N. A. Ottinger and Z. G. Liu, *Appl. Catal., B*, 2014, **160**, 1–9.
15 I. Song, H. Lee, S. W. Jeon, I. A. M. Ibrahim, J. Kim, Y. Byun, D. J. Koh, J. W. Han and D. H. Kim, *Nat. Commun.*, 2021, **12**, 901.
16 R. Y. Qu, D. Ye, C. H. Zheng, X. Gao, Z. Y. Luo, M. J. Ni and K. F. Cen, *RSC Adv.*, 2016, **6**, 102436–102443.
17 D. Ye, R. Y. Qu, H. Song, C. H. Zheng, X. Gao, Z. Y. Luo, M. J. Ni and K. F. Cen, *RSC Adv.*, 2016, **6**, 55584–55592.
18 Z. Y. Fan, J. W. Shi, C. H. Niu, B. R. Wang, C. He and Y. H. Cheng, *Chem. Eng. J.*, 2020, **398**, 125572.
19 D. Ye, R. Y. Qu, C. H. Zheng, K. F. Cen and X. Gao, *Appl. Catal. A*, 2018, **549**, 310–319.
20 J. W. DePalma, D. J. Doren and M. V. Johnston, *J. Phys. Chem. A*, 2014, **118**, 5464–5473.
21 Y. Liske, S. Kapila, V. Flanigan, P. Nam and S. Lorbert, *J. Hazard. Subst. Res.*, 1999, **2**, 1–17.
22 Y. X. Chen, C. Li, J. X. Chen and X. F. Tang, *Environ. Sci. Technol.*, 2018, **52**, 11796–11802.
23 J. Yu, E. Zhang, L. Wang, Z. Song, F. Kong, Y. Ma, H. Zhao and L. Sun, *Energy Fuels*, 2020, **34**, 2107–2116.
24 J. R. Thøgersen, T. Slabiak and N. White, *Ammonium bisulphate inhibition of SCR catalysts*, Haldor Topsøe Inc, Frederikssund, 2007.
25 H. H. Phil, M. P. Reddy, P. A. Kumar, L. K. Ju and J. S. Hyo, *Appl. Catal., B*, 2008, **78**, 301–308.
26 D. Liu, C. Wang, Y. Yu, B.-H. Zhao, W. Wang, Y. Du and B. Zhang, *Chem*, 2019, **5**, 376–389.
27 N. C. Jeong, J. S. Lee, E. L. Tae, Y. J. Lee and K. B. Yoon, *Angew. Chem., Int. Ed.*, 2008, **47**, 10128–10132.
28 D. Ye, R. Y. Qu, H. Song, X. Gao, Z. Y. Luo, M. J. Ni and K. F. Cen, *Chem. Eng. J.*, 2016, **283**, 846–854.
29 Z. W. Huang, Y. Y. Du, J. Zhang, X. M. Wu, H. Z. Shen and G. H. Jing, *Environ. Sci. Technol.*, 2019, **53**, 5309–5318.
30 F. Feng, W. Y. Yang, S. Gao, C. X. Sun and Q. Li, *ACS Sustainable Chem. Eng.*, 2018, **6**, 6166–6174.
31 S. Wendt, P. T. Sprunger, E. Lira, G. K. H. Madsen, Z. S. Li, J. Ø. Hansen, J. Matthiesen, A. Blekinge-Rasmussen, E. Lægsgaard, B. Hammer and F. Besenbacher, *Science*, 2008, **320**, 1755–1759.
32 N. Doudin, G. Collinge, P. K. Gurunathan, M. S. Lee, V. A. Glezakou, R. Rousseau and Z. Dohnalek, *Proc. Natl. Acad. Sci. U. S. A.*, 2021, **118**, e2017703118.
33 M. Lazzeri, A. Vittadini and A. Selloni, *Phys. Rev. B: Condens. Matter Mater. Phys.*, 2001, **63**, 155409.
34 S. F. Guo, Z. W. Huang, L. P. Wang, X. M. Wu, H. Z. Shen and G. H. Jing, *J. Hazard. Mater.*, 2021, **418**, 126289.
35 L. Dall'Acqua, I. Nova, L. Lietti, G. Ramis, G. Busca and E. Giamello, *Phys. Chem. Chem. Phys.*, 2000, **2**, 4991–4998.
36 M. T. Greiner, M. G. Helander, W. M. Tang, Z. B. Wang, J. Qiu and Z. H. Lu, *Nat. Mater.*, 2011, **11**, 76–81.
37 H. C. Hu, I. E. Wachs and S. R. Bare, *J. Phys. Chem.*, 1995, **99**, 10897–10910.

38 F. Giraud, C. Geantet, N. Guilhaume, S. Loridant, S. Gros, L. Porcheron, M. Kanniche and D. Bianchi, *Catal. Today*, 2021, **373**, 69–79.
39 A. Goypiron, J. Devillepin and A. Novak, *J. Raman Spectrosc.*, 1980, **9**, 297–303.
40 G. Z. He, Z. H. Lian, Y. B. Yu, Y. Yang, K. Liu, X. Y. Shi, Z. D. Yan, W. P. Shan and H. He, *Sci. Adv.*, 2018, **4**, eaau4637.
41 I. Song, H. Lee, S. W. Jeon, T. Kim and D. H. Kim, *Chem. Commun.*, 2020, **56**, 15450–15453.
42 E. C. Gentry and R. R. Knowles, *Acc. Chem. Res.*, 2016, **49**, 1546–1556.

Published on 01 novembris 2021. Downloaded on 31.07.2024 03:51:10.


This journal is © The Royal Society of Chemistry 2022